The Protein Journal (2019) 38:134–141
https://doi.org/10.1007/s10930-019-09812-z

Effects of Orientation on the Stability and Affinity of Antibody–GNP Conjugation

Fatemeh Ramezani[1]

Published online: 25 February 2019

Abstract
In medicine, gold nanoparticles are widely used because of its unique properties. They are usually attached to a monoclonal antibody in treatment and diagnosis. Computational and laboratory work has demonstrated that the structure of the protein can change after interaction with gold nanoparticle and the effect of nanoparticle on the protein is dependent on the type of bond between them. Thus, finding out how nanoparticles affect the protein structure can help us to design the optimal complex of gold nanoparticle–antibody. In the present study, docking and molecular dynamic simulation were performed to obtain an insight at the molecular level in the binding of immunoglobulin G to the Gold nanoparticles, the structure change in immunoglobulin G, and binding energies of Fab and Fc domains of Immunoglobulin G to the GNP. We found the Fab region was more stable than the Fc region when bound to the GNP surface and it also had less structural changes. In neutral pH, Van der Waals interactions contribute more to the Fab–GNP interaction compared to electrostatic interactions; However, in Fc–GNP interaction, the main contributor is the electrostatic energy.

Keywords Gold nanoparticle · Immunoglobulin G · Binding energy · Stability

1 Introduction

Owing to their biocompatibility, facile bio-conjugation, and their distinctive optical properties, gold nanoparticles (GNPs) are widely used for gene and drug delivery, nuclear targeting, biomedical diagnosis, immunoassay, and therapeutics [1–6]. Due to their widespread use in various fields such as biology, physics, and chemistry, the interaction between biomolecules and solids surfaces—in particular nanoparticles—have attracted significant attention over the past few decades [7].

Different peptides, proteins, and polymers, etc., have been used for functionalization of GNPs. Antibodies (Abs) are widely used as detection elements and Abs–GNPs conjugates, due to their specific affinities to the target antigens—have drawn more attractions [1, 8–13]. Abs–GNPs conjugations are used as effective agents for diagnostic and therapeutic applications [14].

Computational simulations and experiments have demonstrated that the structure and function of peptide and proteins can change upon interaction with GNPs [15–19]. Various factors such as peptide length [20], protein secondary structure (alpha helix or beta sheath) [18, 21], and protein orientation [21–24] can affect the amount of the change. It is proven that misfolded proteins lack a natural biological activity. Therefore, it is very important to monitor structural changes of protein caused by conjugation to nanoparticles (NP) [15].

The amount of structural changes in the protein varies in binding to different nanoparticles [20].

In 2010, Douglas et al. examined the conformational changes in human blood proteins, histone, fibrinogen, albumin, γ-globulin, and insulin when adsorbed onto GNP using circular dichroism (CD) measurements and fluorescence emission spectroscopy. CD demonstrated that the severity of conformational changes can be strongly altered by the type of protein [15].

In 2012, Kaur et al. found that IgG was absorbed in a sphere with a diameter of ≥ 20 nm and did not bind to protein A. This study showed that the size of the nanoparticles can greatly affect the binding activity of the adsorbed proteins [16].

✉ Fatemeh Ramezani
Ramezani.f@iums.ac.ir

[1] Physiology Research Center, Faculty of Medicine, Iran University of Medical Sciences, Tehran, Iran

In the latest work of our team in 2015, the interaction of human serum albumin with gold nanoparticles and changes in protein structure were investigated using molecular dynamics coupling and simulation. The results showed that after albumin absorption on the gold nanoparticle, human serum albumin was dendrobated and the alpha-helix value was significantly reduced [18].

In a study by Dominguez-Medina et al. in 2016, different interaction pathways between gold nanorods and bovine serum albumin were identified. It was found that bovine serum albumin tolerated local structural changes that affect nanoparticle stability, cancer cell uptake, and even protein secondary structure [17].

In 2014, Zhang et al. found that IgG type protein appears to displace the citrate ligands to bind with the metal core during its interaction with the citrate-coated GNP.

Despite the widespread use of antibody–GNPs complexes, there is no study so far that shows how nanoparticles affect the structure of antibodies? And how is antibody binding more stable? In the present study, we investigated the interaction of human immunoglobulin G (IgG) with gold nanoparticle surface. Research has shown that immunoglobulin, for binding to a gold nanoparticle containing a coating such as citrate, shrinks the coating, and binds to the gold surface [25]. With this in mind, the direct binding of nanoparticles on the surface of gold is considered in this study.

IgG molecules are almost Y-shaped with three parts equal in size which are loosely connected to one another by a flexible belt. The two upper arms are called Fab and the bottom one is called Fc. Areas of Fab that differ in various antibody molecules are called V regions, which participate in binding to the antigen, whereas the Fc region has fewer variations and interacts with molecules and cells. The present study was conducted in order to improve our understanding of IgG structural changes, binding energy of Fc and Fab while binding to the GNP.

2 Computational Method

2.1 Docking of IgG–GNP

We used Auto Dock tools 1.5.4 Application (ADT) to calculate the rigid docking of IgG–GNP [26]. We also used X-ray crystallographic structure of an intact IgG1 monoclonal antibody (PDB accession 1IGY) as the original structure of IgG.

In the present study, by using the term "GNP," we mean cubic gold nanoparticles—gold nanospheres and gold nanorods. We study whether a GNP with an exposed Au (111) face can be considered as a large crystalline surface. If the nanoparticles have a 5-nm diameter (the minimum gold nanosphere size Sigma-Aldrich sells) therefore the accessible space on the surface of an individual nanoparticle is roughly eight times larger than the area occupied by a single protein and if the diameter reaches 10 nm, it is 26 times larger. Therefore, it can be reasonably accepted that IgG views the gold nanosphere as a local flat Au surface [27].

We used the HyperChem program to construct one layer of gold slab from atoms of gold for docking and a five-layer gold for molecular dynamic simulation. For the docking simulation, we considered IgG as a receptor and counted an Au layer with 140 atoms as a ligand. We also considered the active bonds of the ligand to be non-rotating.

2.2 Molecular Dynamic Simulation

We used the molecular dynamics method to simulate the interaction between nanoparticle and antibody. We put the complex in solvent with the TIP3P model of water [28, 29]. The boundary conditions were periodically applied throughout the system. In order to simulate the physiological conditions in the simulation environment, the Cl^- and Na^+ ions with 150 mM concentration were added to the simulation box which eventually neutralized the environment of the box.

We used Gromacs 5.0.6 software package [30–35] and the GolP-CHARMM force field [36] to perform all these simulations. GolP-CHARMM is a force field for gold which is compatible with existing bio-organic force fields such as CHARMM, and predicts the equilibrium of peptide uptake from computational simulations [36].

In the present study, we considered the polarization of gold atoms as an ensemble of hard rods by replacing any of the gold atoms with a dipole with two opposing charges. The protein atom's partial charge forces the rod to an energetically preferential direction, and the average bipolar moment of the rod ranges from zero to a finite value. Additionally, for each gold atom on the surface of Au (111), two LJs (Lnarad Jones) virtual sites (VS), which were located in a hollow place, were created, and using VS, it was possible to attract atoms to the on-top location, which is the actual interaction site instead of the hole. The main gold atoms of the surface were given no LJ interaction. Using the following function, we can calculate the potential energy for interaction between biomolecules and the gold surface:

$$V^{\text{tot}}_{\text{Au}-X} = V^{\text{im}}_{\text{Au}-X} + V^{\text{Chemisorb}}_{\text{Au}-X} + V^{\pi}_{\text{Au}-X}, \quad (1)$$

where $V^{\text{im}}_{\text{Au}-X}$, is the Coulombic electrostatic interaction between the biomolecule and the image charges that induces

in the gold after adsorption; V_{Au-X}^{VDW}, $V_{Au-X}^{Chemisorb}$, and V_{Au-X}^{π} are the interactions of Van der Waals, chemisorption, and π electron between the gold and biomolecule. The 12–6 LJ potentials are used to describe Van der Waals interactions (Eq. 2).

$$V^{vdW}(r_{ij}) = 4\varepsilon_{ij}\left[\left(\frac{\sigma_{ij}}{r_{ij}}\right)^{12} - \left(\frac{\sigma_{ij}}{r_{ij}}\right)^{6}\right], \quad (2)$$

where $\left(\sigma_{ij} = (\sigma_i + \sigma_j)/2,\ \varepsilon_{ij} = (\varepsilon_i \times \varepsilon_j)^{1/2}\right)$.

In addition to the general parameters of the LJ for gold that reproduces the adsorption energy of alkane, the LJ terms for Au–S, Au–N, Au–O, Au–H(–O), and C for chemical species and SP^2 hybridized carbon are set in this force field.

Minimization was performed for 2 ns in the NPT ensemble to remove overlaps between water and amino acids, followed by dynamic simulation for 80 ns in NVT ensemble at $T = 300$°K. Nose–Hoover thermostat [37] was applied to keep the system at optimal temperature. The LINCS algorithm was run to allow a time step of 8×10^{-4} ps [31]. Long-range electrostatic interactions were considered using the Ewald method, with a real space cut-off of 4 Å. Van der Waals interrupted at 14 Å. Visual molecular dynamics (VMD) 1.9 [38] was used to prepare snapshots.

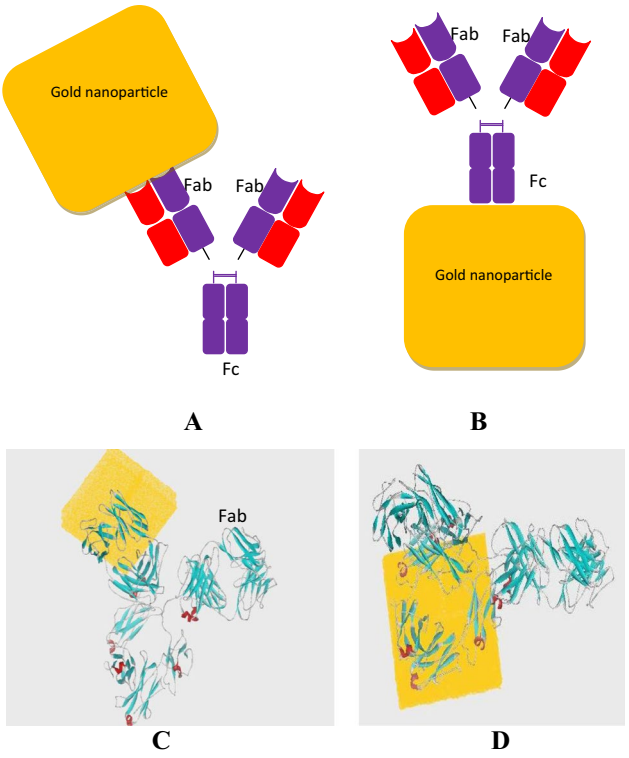

Fig. 1 Main structures of GNPs–IgG interactions through: Fab (**a**) and Fc (**b**) with schematic, and ribbon Fab (**c**), Fc (**d**) representation

3 Results

3.1 Two IgG Orientations on the GNPs from Docking

We performed IgG–GNP docking and chose the complexes that had the highest binding energy score (− 10.3 kcal mol^{-1} for the first complex and − 11 kcal mol^{-1} for the second complex) for the Molecular dynamics simulation (Table 1). Free binding energy = final intermolecular energy + final total internal energy + torsion-free energy unbound system's energy. The unbound system energy and total internal energy are equal and cancel out each other in the free energy equation. Due to ligand's non-rotatable bonds, the torsional-free energy was 0, therefore the free binding energy equals the intermolecular energy. The two structures selected for the molecular dynamic simulation are illustrated in Fig. 1: in one structure, the antibody binds to the GNP from Fab (Fig. 1a, c) and from Fc in the other one (Fig. 1b, d).

3.2 Conformational Changes of IgG upon Binding to the GNPs

After the gold nanoparticle was attached to IgG, in the Fab region which was in direct contact with the GNP, the beta sheet and coil values reached from 42% and 24% to 30% and 34.7%, respectively (Fig. 2a). And as for the Fc region,

Table 1 Encountered complexes resulting from the rigid-body docking of IgG to the GNP surface

	Final intermolecular energy (vdW + H-bond + desolv energy) (1)	Final total internal energy (2)	Unbound system's energy (3)	Estimated free energy of binding = [(1) + (2) − (3)]	Population
Complex 1	− 11	− 7.23	− 7.23	− 11	51
Complex 2	− 10.3 kcal mol^{-1}	− 1.35 kcal mol^{-1}	− 1.35 kcal mol^{-1}	− 10.3 kcal mol^{-1}	44

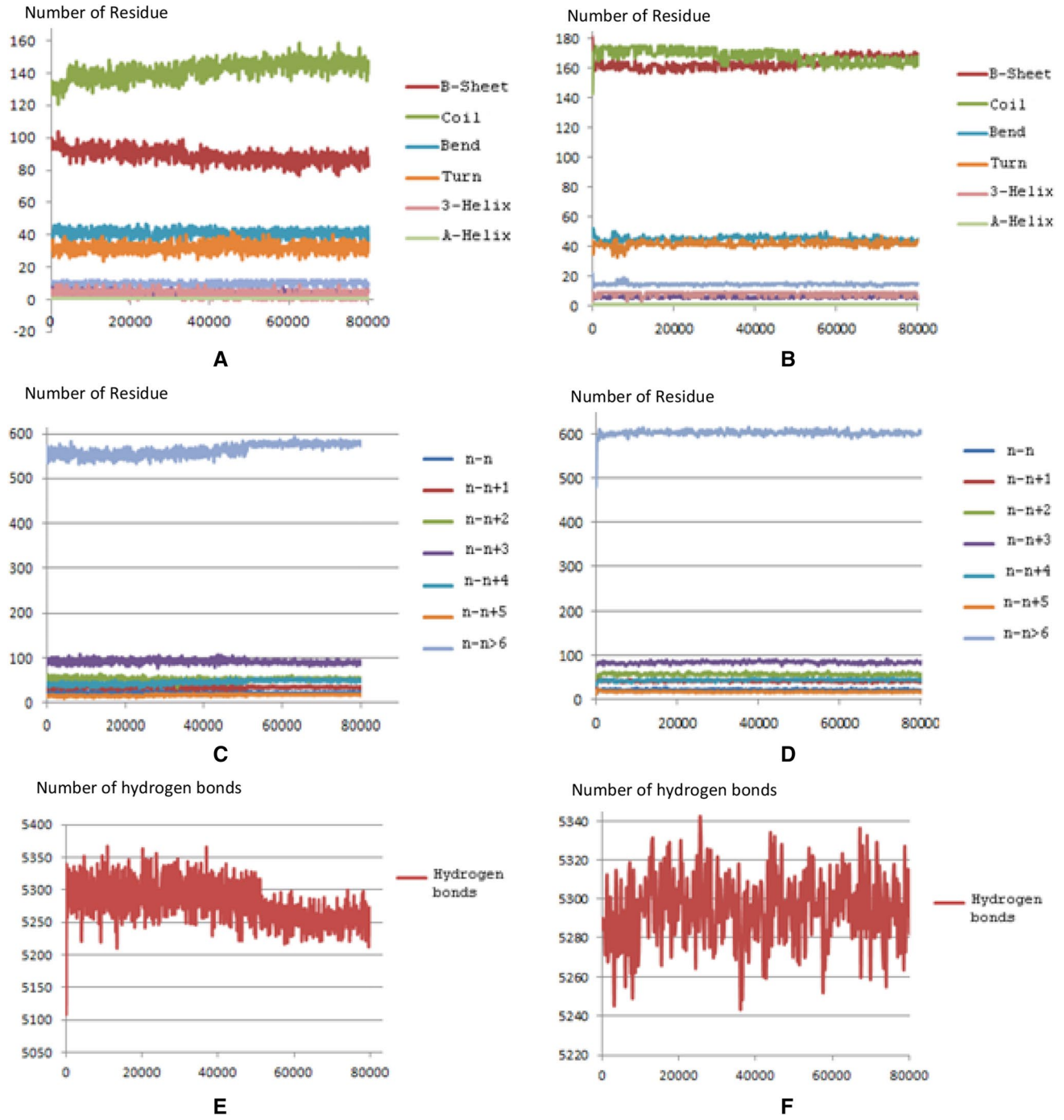

Fig. 2 Changes in the secondary structure components during binding through Fab (**a**) and Fc (**b**), the number of $n-n+x$ $(0 \leq X)$ bonds (from Fab (**c**), from Fc (**d**)) and the number of hydrogen bonds (from Fab (**e**), from Fc (**f**)) on the nanoparticle surface during antibody adsorption

which was in contact with the GNP, the beta sheet values rose by 5.8%, but the amount of coils declined by 6.1% (Fig. 2b).

In the Fab region–GNP bond, the number of bonds between atoms $n - n+x$ $(0 \leq X)$ in Fab domain changed considerably (Fig. 2c) but in Fc region–GNP bond, the number of intra-molecular bonds do not show any major changes (Fig. 2d).

There was a change in the number of hydrogen bonds in IgG upon adsorption into the GNP. The number of hydrogen

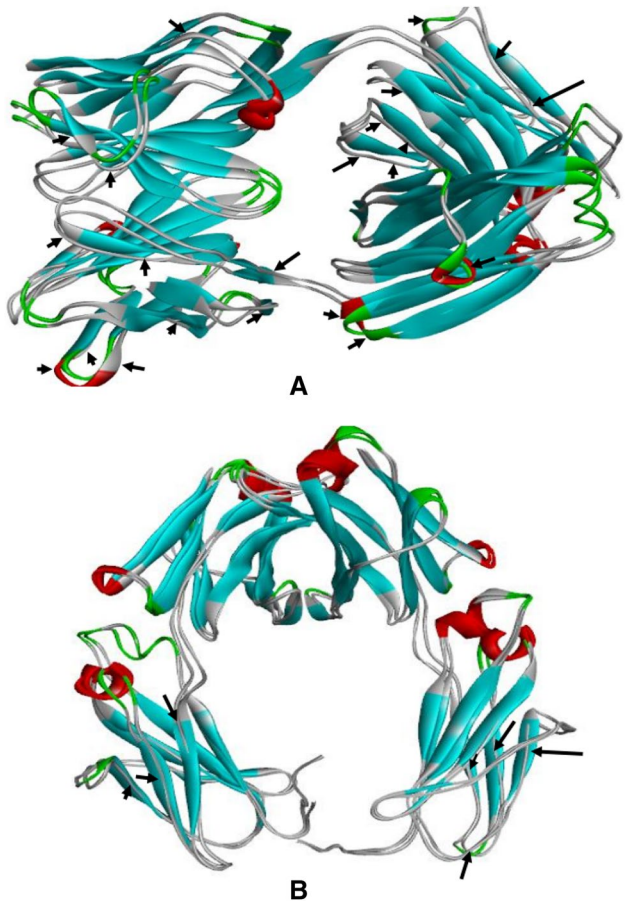

Fig. 3 Superimpose of the two regions Fab (**a**) and Fc (**b**) from IgG before and after the interaction with the gold surface

bonds in Fab-bound IgG decreased. As we mentioned earlier, adsorption of Fab leads to a decrease in the number of beta-sheets but increases the amount of coils. Thus, it seems completely logical for hydrogen bonds to decline in number (Fig. 2e). However, the number of hydrogen bonds to the Fc slightly increased (Fig. 2f).

In Fig. 3, the structure of the immunoglobulin molecule before binding to the GNP and after binding is superimposed, and structural changes are shown in different parts of the molecule. Figure 4 shows the secondary structure of IgG before and after binding to the GNP. The figure demonstrates the changes in secondary structure using amino acids sequence. Each type of secondary structure is illustrated by a different color, so it is easy to distinguish a change in the type of secondary structure. Color key: green–yellow–dark yellow–purple–pink–red–white denotes turn, β sheet, beta bridge, α helix, 3–10 helix, Pi-helix, and coil, respectively.

This figure visually shows the stable and non-stable patterns of secondary structures throughout the trajectories during adsorption on the GNP. By comparing the changes in secondary structure between Fc interactions with GNP during simulation, we found that in a stretch of residues (267–323 and 375–474), there was a major transition with turn turning into beta sheet (transition from green to yellow). We observed the transition for residues (2–206) at the Fab region (transition from yellow to white).

3.3 Binding Energy of IgG–GNP

We calculated the free interaction energies of Fab–GNP (Fig. 5a) Fc–GNP (Fig. 5b) and also the contribution of binding energy by amino acids based on MM-PBSA method (Molecular Mechanics-Poisson–Boltzmann Surface Area) using g_mmpbsa v5.1.2 tool (g_mmpbsa: a GROMACS tool for high-throughput MM-PBSA calculations—PubMed—NCBI). Trajectory frames obtained by MD simulation were used in MM-PBSA method. Fab–GNP binding energy was -250 kj mol^{-1} and with Fc–GNP binding energy was -150 kj mol^{-1}. In the Fc–GNP bond, electrostatic energy was stronger than Van der Waals but in the Fab–GNP bond, Van der Waals energy was higher than the electrostatic energy. As shown in the Fab domain in Fig. 5c, Ala196, Tyr186, Arg155, Gly152 Ala25, and Ser26, have the most negative binding energy to the GNP. In the Fc–GNP bond, Gln1200, Ser1800, Lys1177, Asn1162, Asp1124, Trp1158, and Val1127 have the most negative energy (Fig. 5d).

4 Summary and Conclusions

In immunoassay, the orientation of proteins, particularly antibodies stabilized on GNP surfaces, has an important role. The sensitivity of the methods of diagnosis is dependent on the type of binding between the antibodies and the surface.

Results from the molecular dynamic simulation and docking demonstrate that antibodies attached to the GNP surface with Fab will see more changes in structure compared to when connected to Fc. However, IgG remains almost intact secondary structure-wise when it is adsorbed on to the GNP through Fc. We can conclude that binding of GNP to the

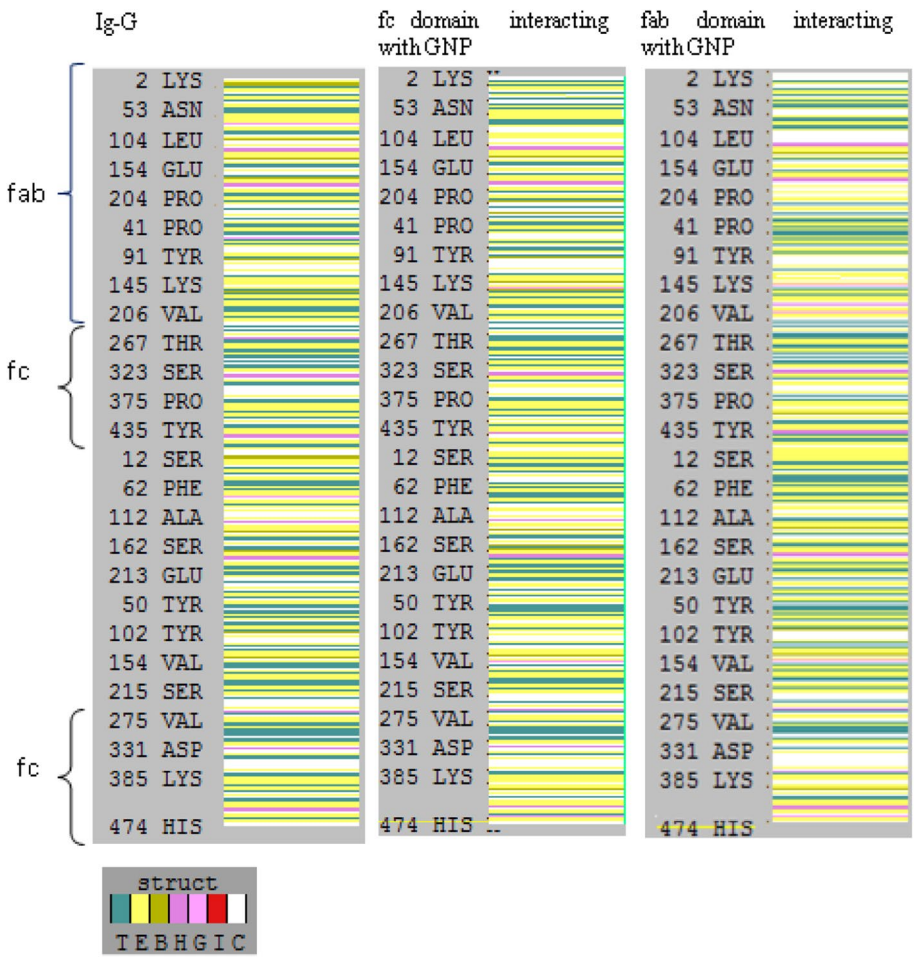

Fig. 4 IgG's secondary structure before (left) and after binding to the GNPs from Fab (middle) and Fc (right). Color key green–yellow–dark yellow–purple–pink–red–white denotes turn, β sheet, beta bridge, α helix, 3–10 helix, Pi-helix, and coil, respectively. (Color figure online)

Fab region caused the structure of IgG molecules to change locally.

If it requires having a stronger antibody-to-surface bond, the antibody must be connected to the surface through the Fab region. As demonstrated in Fig. 5a, b, the Fab region binds with energy of − 250 kj mol^{-1} and the Fc region is bound through − 150 kj mol^{-1} energy. Therefore, binding of Fab to the GNP surface is much more stable than Fc.

In neutral pH, Van der Waals interactions contribute more to Fab–GNP binding compared to electrostatic interactions, but it is the electrostatic energy that plays the key role in Fc–GNP binding. Electrostatic interactions depend on the surrounding pH, therefore it seems like the IgG–Fc binding stability also depends on the pH. These effects can be important in nanoparticle-based cancer treatment, provided that in tumors, the cell membrane pH gradient can reach one unit of pH [25].

This study has been done using molecular dynamics simulation. There are currently no experimental studies in detail showing local structural changes in Abs after binding to the GNP, as well as the effect of Abs orientation on binding stability, to compare the results of the calculations with that. It is hoped that this study will lead to Abs–GNP immobilization/conjugation assessment experiments using analytical methods such as UV–Visible spectroscopy, SPR base assays, or Dynamic light scattering (DLS) to compare the experimental results with the results of computer studies.

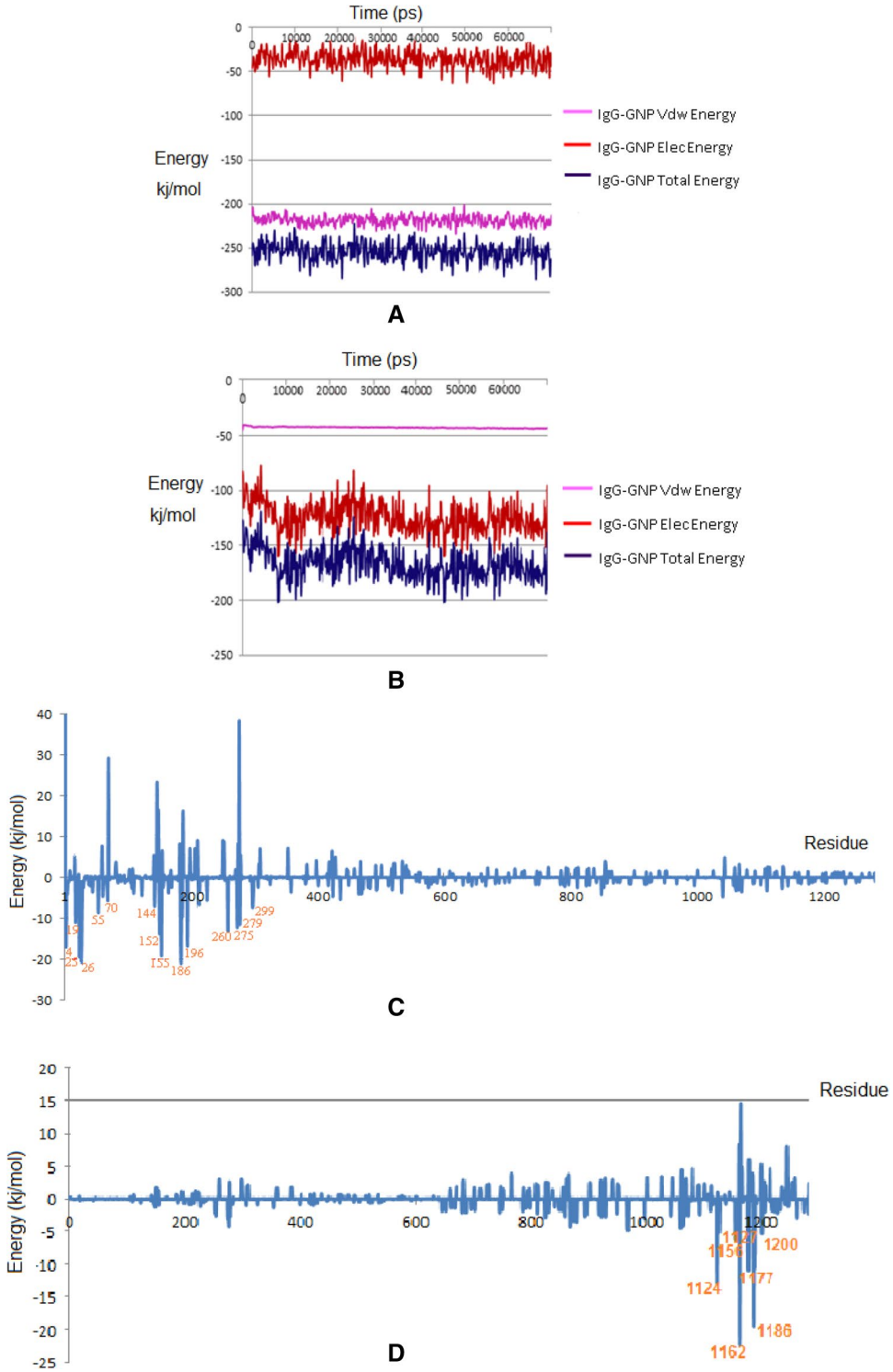

Fig. 5 **a** Fab–GNP binding energy and the contribution by Columbus energy and Vander Der Waals in total binding energy, **b** Fc–GNP Binding energy and the contribution by Columbus energy and Vander Der Waals in total binding energy. **c** Amino acids contribution in binding energy for Fab–GNP interaction, **d** amino acids contribution in binding energy for Fc–GNP interaction

Funding This work has been supported by the IRAN University of Medical Sciences (grant number 31520) and the School of Biological Sciences, Institute for Research in Fundamental Sciences (IPM), Tehran, IRAN.

Compliance with Ethical Standards

Conflict of interest The authors declare that they have no conflict of interest.

Ethical Approval This article does not contain any studies with human participants or animals performed by any of the authors.

References

1. Pham VD, Hoang H, Phan TH, Conrad U, Chu HH (2012) Production of antibody labeled gold nanoparticles for influenza virus H5N1 diagnosis kit development. Adv Nat Sci Nanosci Nanotechnol 3(4):045017
2. Ramezani F (2012) Protein bands detection by nanoparticles after paper chromatography. Int J Nanosci Nanotechnol 8(3):181–184
3. Matijević E (2011) Fine particles in medicine and pharmacy. Springer, New York
4. Huang X, El-Sayed MA (2010) Gold nanoparticles: optical properties and implementations in cancer diagnosis and photothermal therapy. J Adv Res 1(1):13–28
5. Austin LA, MacKey MA, Dreaden EC, El-Sayed MA (2014) The optical, photothermal, and facile surface chemical properties of gold and silver nanoparticles in biodiagnostics, therapy, and drug delivery. Arch Toxicol 88(7):1391–1417
6. Chen ZP et al (2007) A sensitive immunosensor using colloidal gold as electrochemical label. Talanta 72(5):1800–1804
7. Ozboyaci M, Kokh DB, Wade RC (2016) Three steps to gold: mechanism of protein adsorption revealed by Brownian and molecular dynamics simulations. Phys Chem Chem Phys 18(15):10191–10200
8. Wang H, Dimitrov K (2011) Conjugation of immunoglobulin M to gold nanoparticles. Curr Nanosci 7(6):874–878
9. Bailes J, Mayoss S, Teale P, Soloviev M (2012) Gold nanoparticle antibody conjugates for use in competitive lateral flow assays. Methods Mol Biol 906:45–55
10. Yin L, Yang Y, Wang S, Wang W, Zhang S, Tao N (2015) Measuring binding kinetics of antibody-conjugated gold nanoparticles with intact cells. Small 11(31):3782–3788
11. Geng SB et al (2016) Facile preparation of stable antibody-gold conjugates and application to affinity-capture self-interaction nanoparticle spectroscopy. Bioconjug Chem 27(10):2287–2300
12. Ackerson CJ, Jadzinsky PD, Jensen GJ, Kornberg RD (2006) Rigid, specific, and discrete gold nanoparticle/antibody conjugates. J Am Chem Soc 128(8):2635–2640
13. Tan G et al (2015) Conjugation of polymer-coated gold nanoparticles with antibodies—synthesis and characterization. Nanomaterials 5(3):1297–1316
14. Jazayeri MH, Amani H, Pourfatollah AA, Pazoki-Toroudi H, Sedighimoghaddam B (2016) Various methods of gold nanoparticles (GNPs) conjugation to antibodies. Sens Bio-Sens Res 9:17–22
15. De Paoli Lacerda SH et al (2010) Interaction of gold nanoparticles with common human blood proteins. ACS Nano 4(1):365–379
16. Kaur K, Forrest JA (2012) Influence of particle size on the binding activity of proteins adsorbed onto gold nanoparticles. Langmuir 28(5):2736–2744
17. Dominguez-Medina S et al (2016) Adsorption and unfolding of a single protein triggers nanoparticle aggregation. ACS Nano 10(2):2103–2112
18. Ramezani F, Rafii-Tabar H (2015) An in-depth view of human serum albumin corona on gold nanoparticles. Mol BioSyst 11(2):454–462
19. Ramezani F, Amanlou M (2014) Gold nanoparticle shape effects on human serum albumin corona interface: a molecular dynamic study. J Nanoparticle Res 16(7):2512
20. Ramezani F, Habibi M, Rafii-Tabar H, Amanlou M (2015) Effect of peptide length on the conjugation to the gold nanoparticle surface: a molecular dynamic study. DARU J Pharm Sci 23(1):9
21. Mukhopadhyay A, Basu S, Singha S, Patra HK (2018) Inner-view of nanomaterial incited protein conformational changes: insights into designable interaction. Research 2018:1–15
22. Ramezani F, Amanlou M, Rafii-Tabar H (2014) Comparison of amino acids interaction with gold nanoparticle. Amino Acids 46(4):911–920
23. Gagner JE, Lopez MD, Dordick JS, Siegel RW (2011) Effect of gold nanoparticle morphology on adsorbed protein structure and function. Biomaterials 32(29):7241–7252
24. Khan S, Gupta A, Verma NC, Nandi CK (2015) Kinetics of protein adsorption on gold nanoparticle with variable protein structure and nanoparticle size. J Chem Phys 143(16):164709
25. Zhang S, Moustafa Y, Huo Q (2014) Different interaction modes of biomolecules with citrate-capped gold nanoparticles. ACS Appl Mater Interfaces 6(23):21184–21192
26. Johnson N, Frenn M, Feetham S, Simpson P (2011) Autism spectrum disorder: parenting stress, family functioning and health-related quality of life. Fam Syst Health 29(3):232–252
27. Brancolini G, Kokh DB, Wade RC, Corni S (2012) Docking of ubiquitin to gold nanoparticles. ACS Nano 11:9863–9878
28. Mark P, Nilsson L (2001) Structure and dynamics of the TIP3P, SPC, and SPC/E water models at 298 K. J Phys Chem A 105(43):9954–9960
29. Guillot B (2002) Summary for policymakers. In: Intergovernmental Panel on Climate Change (ed) Climate change 2013—the physical science basis, vol 101. Cambridge University Press, Cambridge, pp 1–30
30. Berendsen HJC, van der Spoel D, van Drunen R (1995) GROMACS: amessage-passing parallel molecular dynamics implementation. Comput Phys Commun 91(1–3):43–56
31. Lindahl E, Hess B, van der Spoel D D (2001) GROMACS 3.0: a package for molecular simulation and trajectory analysis. J Mol Model 7(8):306–317
32. van Der Spoel D, Lindahl E, Hess B, Groenhof G, Mark AE, Berendsen HJC (2005) GROMACS: fast, flexible, and free. J Comput Chem 26(16):1701–1718
33. Hess B, Kutzner C, van der Spoel D, Lindahl E (2008) GROMACS 4: algorithms for highly efficient, load-balanced, and scalable molecular simulation. J Chem Theory Comput 4(3):435–447
34. Pronk S et al (2013) GROMACS 4.5: a high-throughput and highly parallel open source molecular simulation toolkit. Bioinformatics 29(7):845–854
35. Abraham MJ et al (2015) GROMACS: High performance molecular simulations through multi-level parallelism from laptops to supercomputers. SoftwareX 1–2:19–25
36. Wright LB, Rodger PM, Corni S, Walsh TR (2013) GolP-CHARMM: first-principles based force fields for the interaction of proteins with Au (111) and Au (100). J Chem Theory Comput 9(3):1616–1630
37. Hünenberger PH (2005) Thermostat algorithms for molecular dynamics simulations. In: Holm C, Kremer K (eds) Advances in polymer science, vol 173. Springer, Berlin, pp 105–149
38. Humphrey W, Dalke A, Schulten K (1996) VMD: visual molecular dynamics. J Mol Graph 14(1):3–38